



Particles II

Access the latest eBook →

11

Advanced
Optical Metrology

Particles II



EVIDENT
OLYMPUS

WILEY

Impact on Biological Systems and the Environment

This eBook is dedicated to the research of Professor David Wertheim.

In collaboration with various groups, Professor Wertheim uses confocal microscopy to analyse the impact of different types of particles on human health and the environment, with a focus on human health-hazardous particles detected with solid-state nuclear track detectors (SSNTD). Download for free, today.

EVIDENT
OLYMPUS

WILEY

Fabrication of Anticounterfeiting Nanocomposites with Multiple Security Features via Integration of a Photoresponsive Polymer and Upconverting Nanoparticles

Yazhi Liu, Shuofeng Liang, Chenrui Yuan, Andreas Best, Michael Kappl, Kaloian Koynov, Hans-Jürgen Butt, and Si Wu*

Anticounterfeiting materials are used to distinguish real banknotes, products, and documents from counterfeits, fakes, or unauthorized replicas. However, conventional anticounterfeiting materials generally exhibit a single anticounterfeiting function, resulting in a low level of security. Herein, a novel anticounterfeiting nanocomposite is demonstrated with numerous prominent security features. The nanocomposite is fabricated by doping upconverting nanoparticles (UCNPs) in a photoresponsive azobenzene-containing polymer (azopolymer). Because of the *cis*–*trans* photoisomerization of the azopolymer, the nanocomposite exhibits photoinduced reversible color changes suitable for anticounterfeiting applications. Additionally, the hard nanocomposite can be converted to a rubber-like soft solid by light irradiation. Imprinted microstructures are fabricated on the photosoftened nanocomposite, which result in photonic colors. Moreover, polarization-dependent structures are fabricated on the nanocomposite via photoinduced orientation for encryption. Importantly, UCNPs in the nanocomposite emit visible light upon excitation by near-infrared light, enabling the observation of various anticounterfeiting structures with high contrast. An advantage of the anticounterfeiting nanocomposite is that the security features can be observed by the naked eye for quick discrimination and can be analyzed using laboratory equipment for higher accuracy. The anticounterfeiting nanocomposite is easily processed on paper, glass, and plastic, which demonstrates its potential anticounterfeiting functions for banknotes, wines, and medicines.

1. Introduction


Counterfeiting is a growing issue worldwide. To combat it, anticounterfeiting materials, such as digital water marks,^[1,2] diffraction gratings,^[3,4] photonic structures,^[5–9] stimuli-responsive materials,^[10–15] and luminescent materials,^[16,17] have been developed for distinguishing banknotes, valuable products, important documents, etc. These anticounterfeiting materials alter their appearance, color, optical signal, or other properties in response to external stimuli,^[1,18] and their responses can be observed by the naked eye or validated using analytical tools, thereby helping distinguish counterfeits from real ones. An issue with traditional anticounterfeiting materials is that they usually have a single security feature, such as a unimodal emission or a color change. Such materials provide a low level of security because the replication of a single security feature is relatively easy. In addition, high-end applications require that anticounterfeiting materials are discerned quickly (by the naked eye) and accurately (by analytical tools). It is possible to label a product with several anticounterfeiting

materials that impart numerous security features to it; however, processing several anticounterfeiting materials on a product is complicated, and step-by-step labeling of different counterfeiting materials has low production efficiency.^[19] To solve the above-mentioned problems, it is necessary to integrate multiple security features, different read-out methods, and easy processing into a single anticounterfeiting material.

In this study, we introduced a novel nanocomposite, which has several prominent security features that can be discerned with the naked eye and using analytical tools. The nanocomposite has good processability and can be easily applied to banknotes, wines, medicines, and other products (**Figure 1a**). It is composed of a photoresponsive azobenzene-containing polymer (azopolymer) and upconverting nanoparticles (UCNPs). Because of reversible *cis*–*trans* photoisomerization,^[20,21] azopolymers show photochromism,^[22] photoswitchable glass transition temperature (T_g) values,^[23] and photoinduced orientations.^[24,25] These photoresponsive properties enable the development of

Y. Liu, S. Liang, C. Yuan, Prof. S. Wu
CAS Key Laboratory of Soft Matter Chemistry
Hefei National Laboratory for Physical Sciences at the Microscale
Anhui Key Laboratory of Optoelectronic Science and Technology
Department of Polymer Science and Engineering
University of Science and Technology of China
Hefei 230026, China
E-mail: siwu@ustc.edu.cn

Y. Liu, A. Best, Dr. M. Kappl, Dr. K. Koynov, Prof. H.-J. Butt, Prof. S. Wu
Max Planck Institute for Polymer Research
Ackermannweg 10, 55128 Mainz, Germany

 The ORCID identification number(s) for the author(s) of this article can be found under <https://doi.org/10.1002/adfm.202103908>.

© 2021 The Authors. Advanced Functional Materials published by Wiley-VCH GmbH. This is an open access article under the terms of the Creative Commons Attribution License, which permits use, distribution and reproduction in any medium, provided the original work is properly cited.

DOI: 10.1002/adfm.202103908

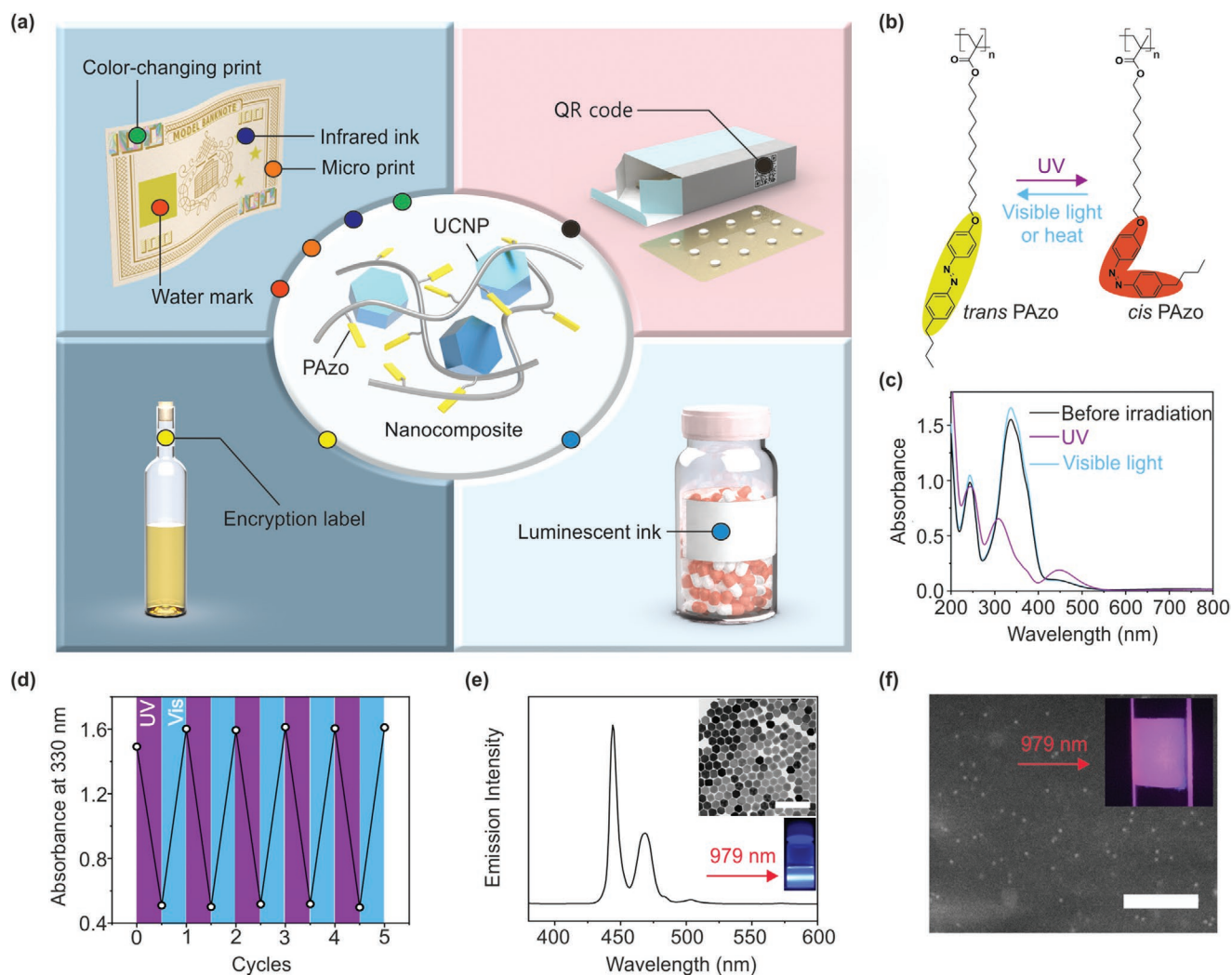


Figure 1. a) Schematic of the anticounterfeiting nanocomposite comprising of the azopolymer (PAzo) and UCNPs for different applications. b) Chemical structure and photoisomerization of PAzo. c) UV-vis absorption spectra of a spin-cast film of PAzo before irradiation, after UV irradiation (365 nm, 67 mW cm⁻², 1 min), and subsequent visible light irradiation (530 nm, 42 mW cm⁻², 1 min). d) The absorption changes under alternating UV and visible light irradiation. e) Upconversion luminescence spectrum ($\lambda_{\text{ex}} = 979$ nm) of β -phase NaYF₄:TmYb@NaYF₄ (core = NaYF₄: 0.5 mol% Tm³⁺/30 mol% Yb³⁺; shell = NaYF₄) UCNPs excited with NIR light (10.8 W cm⁻²). Insets: A TEM image of UCNPs and a photograph of a dispersion of UCNPs upon a 979 nm laser exposure. Scale bar: 200 nm. f) SEM image of PAzo/UCNP nanocomposite. Scale bar: 1 μ m. Inset: A photograph of the nanocomposite on a quartz substrate upon a 979 nm laser exposure.

various anticounterfeiting features, such as color-changing structures, photonic structures, and polarization-dependent structures, on the nanocomposite. UCNPs, which convert near-infrared (NIR) light to visible light,^[26] impart high-contrast color-, structure-, and polarization-dependent upconversion luminescence to the nanocomposite. The synergistic combination of the azopolymer and UCNPs makes the nanocomposite an advanced anticounterfeiting material.

2. Results and Discussion

We synthesized the azopolymer PAzo matrix of the nanocomposite (Figure 1b and Figure S1, Supporting Information). The number-average molecular weight (M_n) and polydispersity index of PAzo measured by gel permeation chromatography

were 3.2×10^4 g mol⁻¹ and 1.12, respectively (Figure S2, Supporting Information). PAzo exhibited reversible *cis-trans* photoisomerization (Figure 1b,c). The spin-cast film of PAzo exhibited a strong π - π^* absorption band at 337 nm and a weak n - π^* band at 448 nm. UV irradiation decreased the π - π^* band intensity and increased the n - π^* band intensity, demonstrating that *cis-trans* isomerization had occurred. According to the absorbance at 330 nm, the *cis* content of azobenzene groups of the nanocomposites film was 70% after UV irradiation. PAzo/UCNP Subsequent visible-light irradiation transformed the *cis* PAzo back to its *trans* state. Reversible photoisomerization was also induced for multiple cycles (Figure 1d).

In addition, β -phase NaYF₄:TmYb@NaYF₄ UCNPs (core = NaYF₄: 0.5 mol% Tm³⁺/30 mol% Yb³⁺; shell = NaYF₄) were synthesized (the Supporting Information). Transmission electron microscopy (TEM) and dynamic light scattering

studies of these UCNPs showed average particle diameters of 53 and 57 nm, respectively (Figure S3, Supporting Information). The UCNPs emitted blue light upon excitation with NIR light at 979 nm (Figure 1e).

To prepare the target nanocomposite, PAzo and UCNPs were mixed in an organic solvent and thin films were prepared by spin-coating or drop-casting. The UCNP content in the nanocomposite was 10 wt%. Scanning electron microscopy (SEM) images of the nanocomposite film showed that a homogeneous material was obtained (Figure 1f and Figure S4, Supporting Information).

To demonstrate the anticounterfeiting function of the nanocomposite, reversible color-changing patterns were fabricated on a nanocomposite film based on *cis-trans* photoisomerization (Figure 2a). Initially, a drop-cast film of the PAzo/UCNP nanocomposite was in a stable *trans* state (Figure 2ai). After the film was irradiated with UV light through a photomask, the irradiated areas changed from yellow to orange due to *cis-trans* isomerization (Figure 2aii) and a pattern was formed. The pattern was then erased via heating, which induced *cis-to-trans* reverse isomerization (Figure 2aiii). Another pattern

was fabricated on the film using a different photomask (Figure 2aiv). Reversible color changes can be easily observed with the naked eye for anticounterfeiting.

We observed that the *trans* PAzo/UCNP nanocomposite was a hard solid, while the *cis* PAzo/UCNP nanocomposite was a soft rubber-like material (Figure 2b). We recently demonstrated that azopolymers exhibit photoswitchable T_g values.^[23] Therefore, we inferred that the PAzo/UCNP nanocomposite also exhibits a photoswitchable T_g , which results in reversible photosoftening. Hence, we examined *trans* and *cis* PAzo/UCNP nanocomposites by dynamic mechanical analysis (DMA). *Trans* PAzo/UCNP had a T_g of 71 °C (Figure 2c). Its storage modulus (G') and loss modulus at temperatures (G'') below T_g were similar to those of plastic; thus, it was a hard solid at room temperature. In contrast, the *cis* PAzo/UCNP nanocomposite was a rubber-like material at room temperature because of its T_g of -11 °C (Figure 2d and Figure S5, Supporting Information).

Photonic structures were imprinted on the photosoftened areas of the PAzo/UCNP nanocomposite (Figure 2e). A spin-cast film of the nanocomposite was irradiated with UV light through

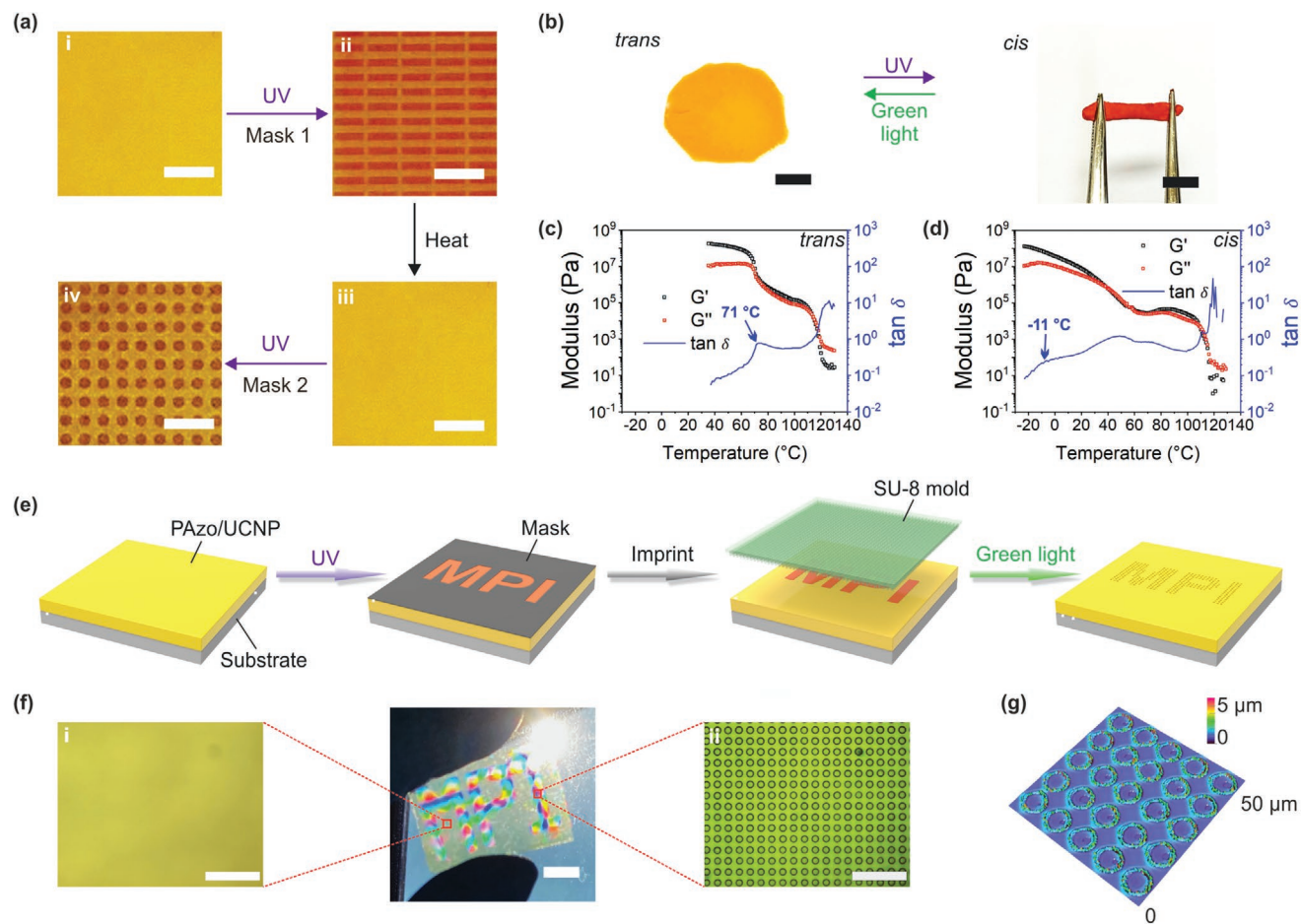


Figure 2. a) Reversible writing and erasure of color-changing patterns on a PAzo/UCNP nanocomposite film. The patterns were fabricated via UV irradiation (365 nm, 67 mW cm⁻², 5 min) through a photomask; patterns were erased via heating (130 °C, 10 min). Scale bars: 5 mm. b) Photographs of *trans* and *cis* PAzo/UCNP nanocomposites. Scale bars: 5 mm. c,d) Dynamic mechanical analysis (DMA) data of c) *trans* and d) *cis* PAzo/UCNP nanocomposites. G' : storage modulus; G'' : loss modulus; $\tan \delta$ loss tangent. e) Schematic of the fabrication of imprinted microstructures with structural colors. f) Photograph of a PAzo/UCNP nanocomposite film with imprinted microstructures on a polyethylene terephthalate substrate. Scale bar: 1 cm. Optical microscopy images of i) an unimprinted area and ii) an imprinted area. Scale bars: 50 μ m. g) Confocal microscopy image of imprinted microstructures on a PAzo/UCNP nanocomposite film.

a photomask. Then, a predesigned photoresist mold (Figure S6, Supporting Information) was pressed on the film (63.7 kPa). After that, the mold was removed and the film was irradiated with green light (530 nm, 58 mW cm⁻², 10 min) to transform it back to its hard solid state. Periodic microstructures of the negative mold were replicated in the irradiated areas (Figure 2fii). The microstructures had a depth of 300 nm (Figure 2g and Figure S7, Supporting Information) and showed vivid structural colors (Figure 2f), which could be used for anticounterfeiting.

Polarization-dependent structures were fabricated on a PAzo/UCNP nanocomposite film for encryption (Figure 3a).

UV irradiation induced *trans-to-cis* isomerization (Figure 3ai,ii). Then, irradiation of the *cis* nanocomposite film with polarized blue light induced the alignment of the azobenzene chromophores (Figure 3aiii), which was confirmed by polarized absorption spectroscopy (Figure 3b). The order parameter of oriented azobenzene chromophores was 0.55, which was calculated by the polarized absorbance. This phenomenon is called photoinduced orientation, which occurs when azobenzene chromophores in an azopolymer film align perpendicular to the polarization direction of the incident linearly polarized light irradiation.^[24,27,28] After that, the film was irradiated with UV light

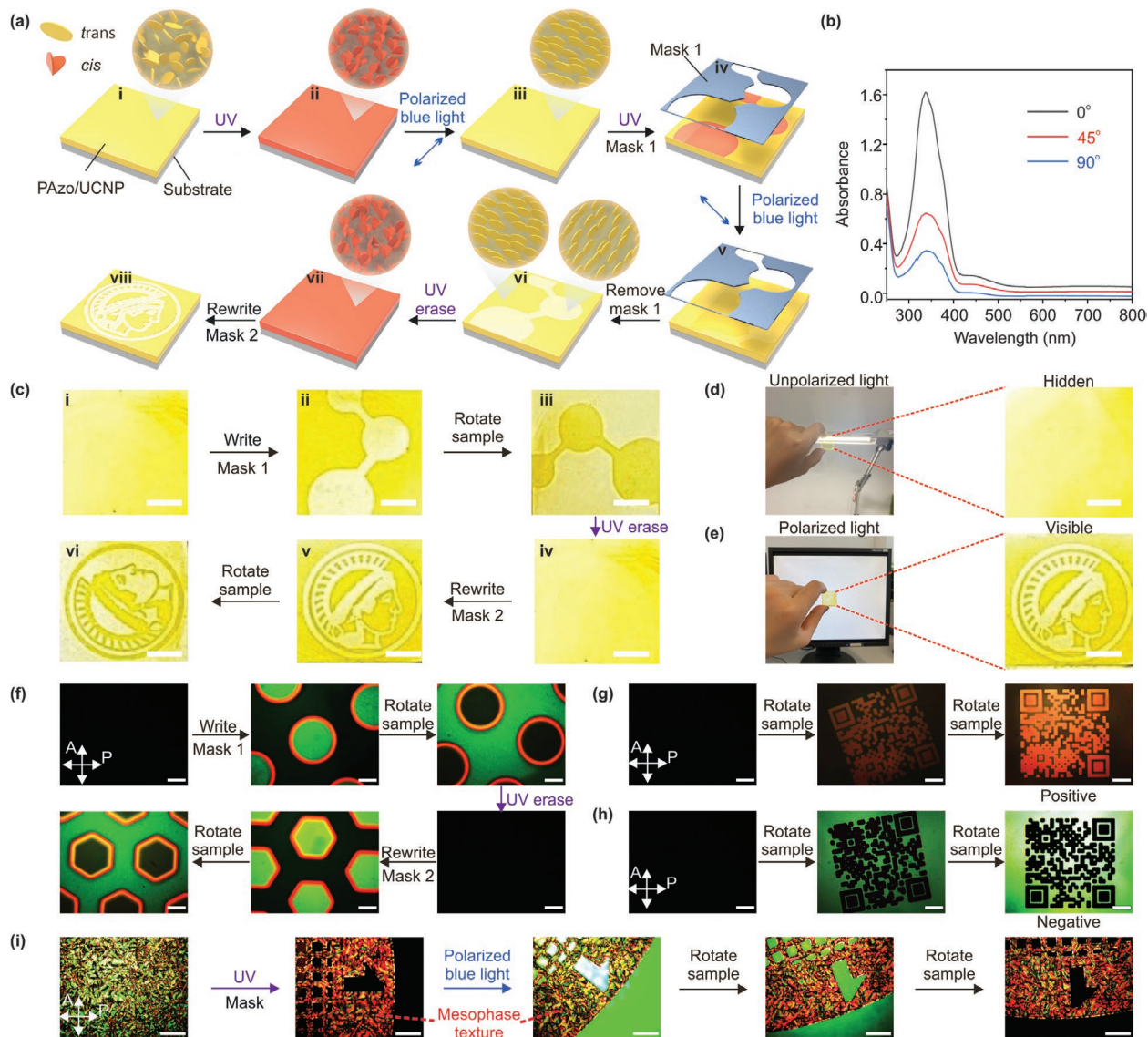


Figure 3. a) Fabrication of rewritable polarization-dependent patterns on a PAzo/UCNP nanocomposite film. b) Polarized absorption spectra of a nanocomposite film after UV (365 nm, 67 mW cm⁻², 10 min) and linearly polarized blue light (470 nm, 29 mW cm⁻², 30 min) irradiations. c) Photographs of a nanocomposite film with rewritable polarization-dependent patterns under polarized light from a monitor. Scale bars: 0.5 mm. d,e) The polarization-dependent pattern was d) invisible under unpolarized light from a desk lamp and e) visible under polarized light from a monitor. Scale bars: 0.5 mm. f) The erasure and rewriting of polarization-dependent patterns on a nanocomposite film observed using polarized optical microscopy (POM). A: analyzer; P: polarizer. Scale bars: 200 μm. g,h) POM images of the positive and negative QR codes on nanocomposite films. Scale bars: 200 μm. i) POM images of a nanocomposite film before irradiation and after UV (365 nm, 67 mW cm⁻², 10 min) and subsequent linearly polarized blue light irradiations (470 nm, 29 mW cm⁻², 30 min) through a photomask.

and polarized blue light through a photomask (Figure 3aiv,v). The polarization direction was perpendicular to the previously polarized blue light; therefore, the azobenzene chromophores in the exposed areas were oriented perpendicular to those in the unexposed areas (Figure 3avi). The pattern was erasable using UV light (Figure 3avii) and rewritable using a different photomask (Figure 3aviii).

A polarization-dependent pattern was observed using polarized light from a monitor (Figure 3c). The light/dark contrast of the pattern was reverted by rotating it by 90° (Figure 3cii,iii) because the transmittance of the polarized monitor light changed. The pattern was erasable and rewritable (Figure 3civ–vi). Moreover, the pattern was hidden under unpolarized light from a desk lamp (Figure 3d), while it was visible under polarized light from a monitor (Figure 3e). Thus, the polarization-dependent pattern allows encryption, which secures it against counterfeiting.

Next, we investigated the resolution of our patterning technique using different photomasks (Figure 3f and Figure S8, Supporting Information). The fabrication of patterns with a pixel size smaller than 10 μm is feasible. Such high-resolution structures make it difficult to replicate anticounterfeiting patterns.

Thus, they meet the standard for high-security applications. To demonstrate the applications of such patterns, we fabricated high-resolution “positive” and “negative” quick response (QR) codes (Figure 3g,h), which stayed intact for more than 180 d in an office with natural light at room temperature (Figure S9, Supporting Information).

The polarization-dependent patterns (Figure 3f–h) have uniformly aligned structures. We imparted an additional security feature to the structures using mesophase textures as fingerprint-like structures (Figure 3i). A pattern with both uniform and textured parts was fabricated by irradiating a nanocomposite film with UV light and polarized blue light through a photomask (Figure 3i). The texture of the unexposed areas was attributed to the mesophases of PAzo (Figure S10 and Figure S11, Supporting Information). Relatively large crystalline grains were formed in the pure PAzo samples, while smaller crystalline grains were formed by the introduction of UCNPs into PAzo, which increased the defects in the mesophase structures (Figure S12, Supporting Information). Thus, the textures of the PAzo/UCNP nanocomposites can be tuned by adjusting the UCNP content.

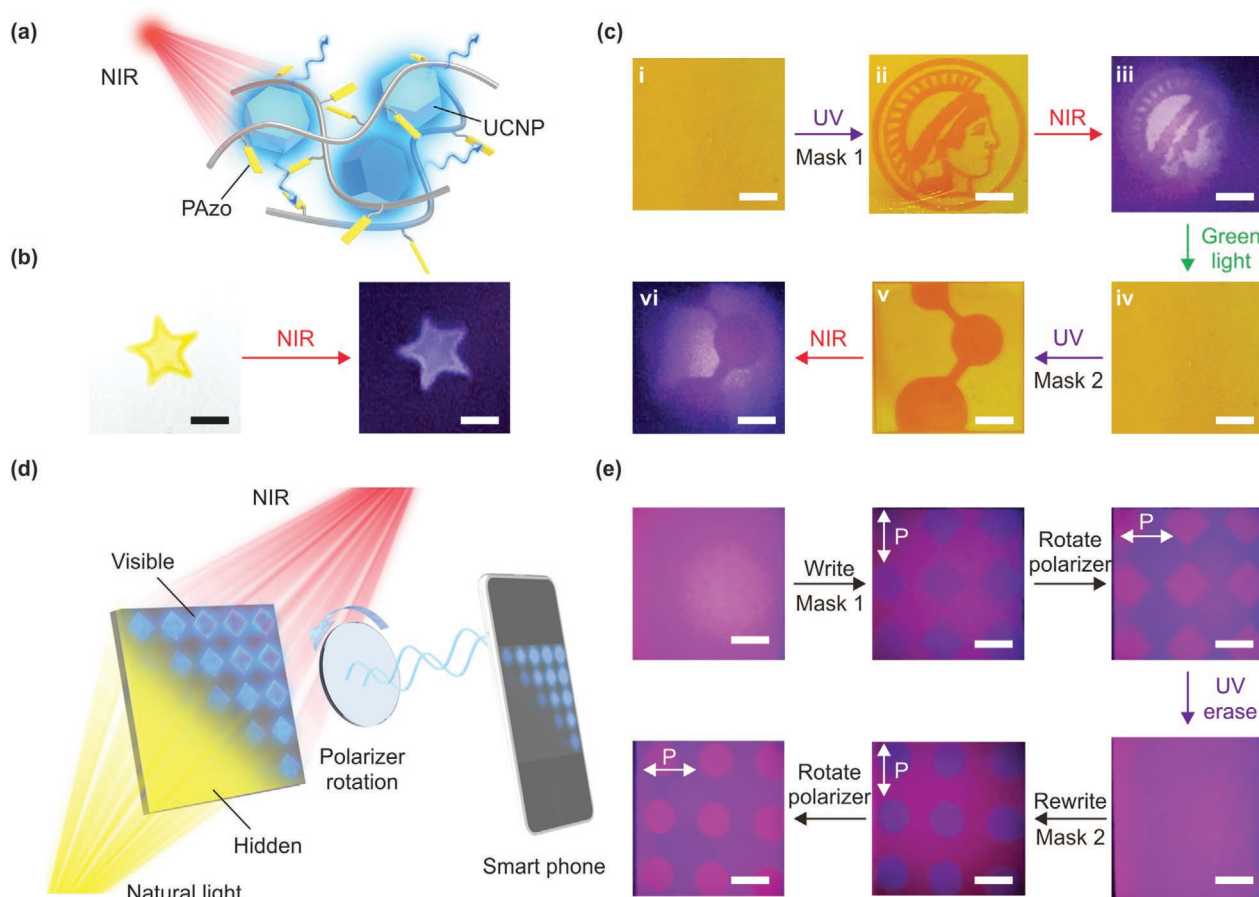


Figure 4. a) Schematic of upconversion luminescence of PAzo/UCNP nanocomposite excited with NIR light. b) Photographs of a star-shaped PAzo/UCNP nanocomposite stamped on a substrate excited with NIR light (10.8 W cm^{-2}). Scale bars: 5 mm. c) Photographs of rewritable photochromic patterns of PAzo/UCNP nanocomposite unraveled using upconversion luminescence. Scale bars: 5 mm. d) Schematic of accessing encrypted information on a polarization-dependent display using upconversion luminescence. e) Photographs of rewritable patterns with polarization-dependent upconversion luminescence. P indicates the polarization direction. Scale bars: 5 mm.

UCNPs emit visible light upon excitation with NIR light, which provides the nanocomposite with a new security feature (Figure 4a). A star-shaped structure made of PAzo/UCNP nanocomposite was stamped on a glass substrate, which exhibited upconversion luminescence (Figure 4b). NIR light irradiation on the film had minor thermal effects, which did not affect the properties of the PAzo/UCNPs nanocomposites (Figure S13, Supporting Information).

Upconversion luminescence was combined with rewritable photochromic patterns. When the photochromic pattern was excited with NIR light, the *trans* PAzo/UCNP part (yellow) emitted stronger upconversion luminescence, while the *cis* PAzo/UCNP part (orange) emitted weaker upconversion luminescence (Figure 4c), because *cis* PAzo absorbed upconversion luminescence (Figure S14, Supporting Information). Therefore, the synergy of UCNPs and PAzo can be used for anticounterfeiting applications.

The PAzo/UCNP nanocomposites showed polarization-dependent upconversion luminescence, which represents a high-end technique for anticounterfeiting (Figure 4d). We fabricated a polarization-dependent pattern on a nanocomposite film via a photoinduced orientation (Figure 3). Polarization-dependent patterns were invisible under natural light (Figure S15a, Supporting Information), but were legible using polarized upconversion luminescence (Figure 4e). The brightness of the polarized upconversion luminescence patterns changed with the rotation of the polarizer. Polarized upconversion luminescence patterns are also erasable and rewritable. Moreover, because excitation by NIR light

avoids fluorescence and light from the background, a weak polarization-dependent pattern (Figure S15b, Supporting Information) was observed using polarized upconversion luminescence (Figure 4e). Thus, these properties can be used for high-contrast patterns and high-quality encryption, which provide a high level of security.

To demonstrate multiple security features, we integrated four anticounterfeiting functions of the PAzo/UCNP nanocomposite on a model banknote (Figure 5a). Structural colors, upconversion luminescence, polarization-dependent patterns, and high-resolution microprints with mesophase textures provide numerous prominent features for anticounterfeiting applications. Furthermore, PAzo/UCNP nanocomposites are also suitable for anticounterfeiting applications for a variety of products. For example, we fabricated a QR code on a medicine box using PAzo/UCNP composites (Figure 5b). In addition, because of their good mechanical properties and processability, PAzo/UCNP composites can be applied to the curved surfaces of wine and capsule bottles (Figure 5c,d and Figure S16, Supporting Information).

3. Conclusion

In conclusion, we developed an anticounterfeiting nanocomposite with multiple security features, different read-out methods, and easy processing. These properties are based on the integration of a photoresponsive azopolymer and UCNPs into the nanocomposite. These nanocomposites can be

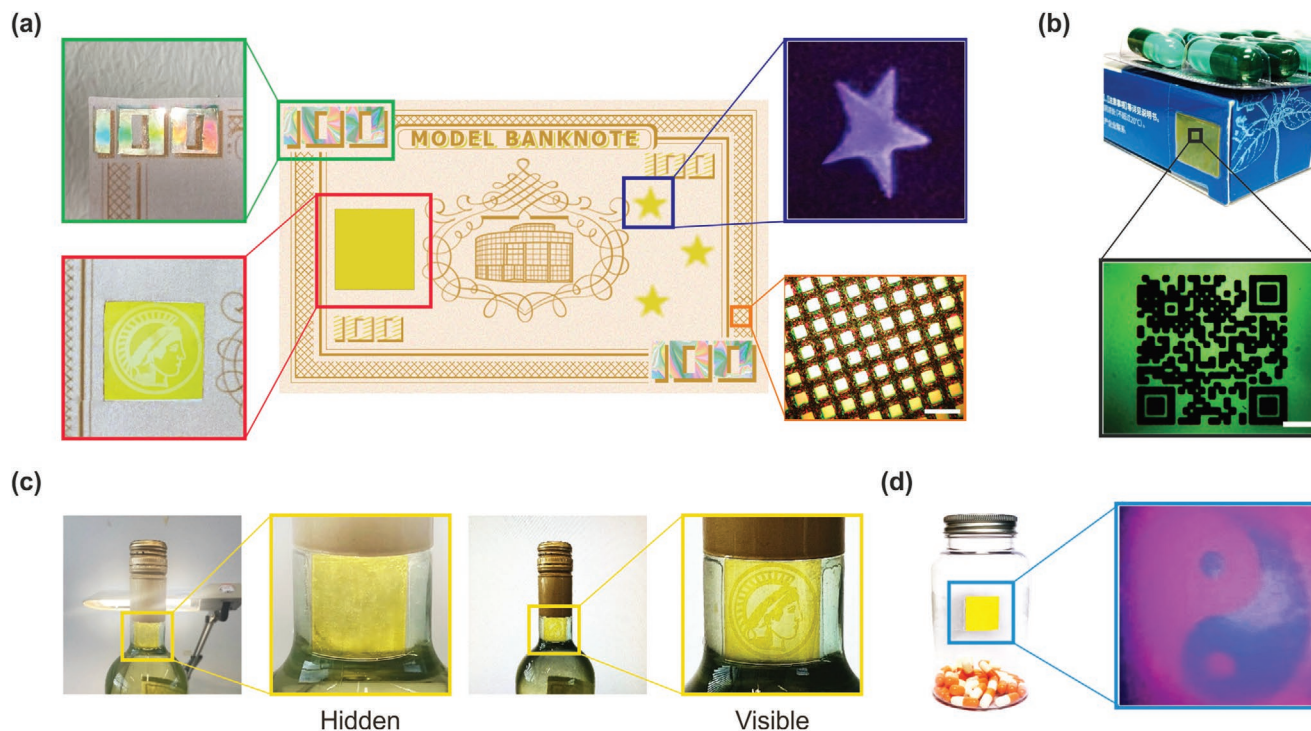


Figure 5. a) The integration of multiple anticounterfeiting functions of PAzo/UCNP nanocomposites in a model banknote. Upper left: structural color, upper right: upconversion luminescence, down left: polarization-dependent pattern, and down right: patterned structures with mesophase textures. Scale bar: 100 μm . b) POM image of a QR code on a medicine box. Scale bar: 200 μm . c) A label on the curved surface of a wine bottle observed under a desk lamp (left) and monitor light (right). d) A label with polarized upconversion luminescence on a curved surface of a bottle under NIR light.

conveniently processed and applied to banknotes, medicines, wines, and other products. The anticounterfeiting structures in the nanocomposite have high resolution, are durable, and can be discerned with the naked eye for quick discrimination and with analytical tools for high accuracy. The results of this study open a new avenue for the development of high-end anticounterfeiting materials.

Supporting Information

Supporting Information is available from the Wiley Online Library or from the author.

Acknowledgements

This work was supported by National Natural Science Foundation of China (NSFC, No. 52073268), the Fundamental Research Funds for the Central Universities (WK3450000006 and WK2060190102), Anhui Provincial Natural Science Foundation (No. 1908085MB38), the Thousand Talents Plan and the Deutsche Forschungsgemeinschaft (DFG, WU 787/8-1). The authors thank G. Schaefer and A. Hanewald (Max Planck Institute for Polymer Research) for their technical support.

Open access funding enabled and organized by Projekt DEAL.

Conflict of Interest

The authors declare no conflict of interest.

Data Availability Statement

The data that support the findings of this study are available on request from the corresponding author.

Keywords

anticounterfeiting, nanocomposites, photoresponsive, polymers, upconverting nanoparticles

Received: April 26, 2021

Revised: May 11, 2021

Published online: June 29, 2021

[1] E. L. Prime, D. H. Solomon, *Angew. Chem., Int. Ed.* **2010**, *49*, 3726.

[2] R. Arppe, T. J. Sørensen, *Nat. Rev. Chem.* **2017**, *1*, 0031.

- [3] Y. Zhao, X. Zhao, M. D. Li, Z. Li, H. Peng, X. Xie, *Angew. Chem., Int. Ed.* **2020**, *59*, 10066.
- [4] G. Babakhanova, T. Turiv, Y. Guo, M. Hendrikx, Q.-H. Wei, A. P. H. J. Schenning, D. J. Broer, O. D. Lavrentovich, *Nat. Commun.* **2018**, *9*, 456.
- [5] A. J. J. Kragt, D. C. Hoekstra, S. Stallinga, D. J. Broer, A. P. H. J. Schenning, *Adv. Mater.* **2019**, *31*, 1903120.
- [6] P. Zhang, G. Zhou, L. T. Haan, A. P. H. J. Schenning, *Adv. Funct. Mater.* **2020**, *31*, 1900789.
- [7] L. Qin, X. Liu, K. He, G. Yu, H. Yuan, M. Xu, F. Li, Y. Yu, *Nat. Commun.* **2021**, *12*, 699.
- [8] A. Priimagi, A. Shevchenko, *J. Polym. Sci., Part B: Polym. Phys.* **2014**, *52*, 163.
- [9] B. Yang, F. Cai, S. Huang, H. Yu, *Angew. Chem., Int. Ed.* **2020**, *59*, 4035.
- [10] J. Feng, F. Yang, X. Wang, F. Lyu, Z. Li, Y. Yin, *Adv. Mater.* **2019**, *31*, 1900789.
- [11] X. Zhou, L. Wang, Z. Wei, G. Weng, J. He, *Adv. Funct. Mater.* **2019**, *29*, 1903543.
- [12] Z. Shi, P. Peng, D. Strohecker, Y. Liao, *J. Am. Chem. Soc.* **2011**, *133*, 14699.
- [13] M. Cheng, Q. Liu, G. Ju, Y. Zhang, L. Jiang, F. Shi, *Adv. Mater.* **2014**, *26*, 306.
- [14] Y. Zheng, M. K. Liong Han, Q. Jiang, B. Li, J. Feng, A. del Campo, *Mater. Horiz.* **2020**, *7*, 111.
- [15] H. Zeng, P. Wasylczyk, D. S. Wiersma, A. Priimagi, *Adv. Mater.* **2018**, *30*, 1703554.
- [16] L. Huang, W. Wu, Y. Li, K. Huang, L. Zeng, W. Lin, G. Han, *J. Am. Chem. Soc.* **2020**, *142*, 18460.
- [17] M. Dietrich, G. Delaittre, J. P. Blinco, A. J. Inglis, M. Bruns, C. Barner-Kowollik, *Adv. Funct. Mater.* **2012**, *22*, 304.
- [18] B. Hardwick, W. Jackson, G. Wilson, A. W. H. Mau, *Adv. Mater.* **2001**, *13*, 980.
- [19] Y. Zheng, C. Jiang, S. H. Ng, Y. Lu, F. Han, U. Bach, J. J. Gooding, *Adv. Mater.* **2016**, *28*, 2330.
- [20] W.-C. Xu, S. Sun, S. Wu, *Angew. Chem., Int. Ed.* **2019**, *58*, 9712.
- [21] X. Tong, M. Pelletier, A. Lasia, Y. Zhao, *Angew. Chem., Int. Ed.* **2008**, *47*, 3596.
- [22] G. S. Kumar, D. Neckers, *Chem. Rev.* **1989**, *89*, 1915.
- [23] H. Zhou, C. Xue, P. Weis, Y. Suzuki, S. Huang, K. Koynov, G. K. Auernhammer, R. Berger, H.-J. Butt, S. Wu, *Nat. Chem.* **2017**, *9*, 145.
- [24] Y. Wu, T. Ikeda, Q. Zhang, *Adv. Mater.* **1999**, *11*, 300.
- [25] J.-A. Lv, Y. Liu, J. Wei, E. Chen, L. Qin, Y. Yu, *Nature* **2016**, *537*, 179.
- [26] B. Yan, J.-C. Boyer, N. R. Branda, Y. Zhao, *J. Am. Chem. Soc.* **2011**, *133*, 19714.
- [27] W. M. Gibbons, T. Kosa, P. Palfy-Muhoray, P. J. Shannon, S. T. Sun, *Nature* **1995**, *377*, 43.
- [28] A. Natansohn, P. Rochon, *Chem. Rev.* **2002**, *102*, 4139.